Monitoring β-cell survival after intrahepatic islet transplantation using dynamic exendin PET imaging: a proof-of-concept study in individuals with type 1 diabetes

Jansen, T.J.P.; Buitinga, M.; Boss, M.; Nijhoff, M.F.; Brom, M.; Galan, B.E. de; ... ; Gotthardt, M.

Monitoring β-Cell Survival After Intrahepatic Islet Transplantation Using Dynamic Exendin PET Imaging: A Proof-of-Concept Study in Individuals With Type 1 Diabetes

Theodorus J.P. Jansen,[1] Mijke Buitinga,[2,3] Marti Boss,[1] Michiel F. Nijhoff,[4] Maarten Brom,[1] Bastiaan E. de Galan,[5,6,7] Marinette van der Graaf,[1] Sebastiaan van Koeverden,[1] Marie-Christine Vantyghem,[8,9] Amandine Beron,[10] François Pattou,[9] Marten A. Engelse,[4] Irina Velikyan,[11] Olof Eriksson,[11] Eelco J.P. de Koning,[4] and Martin Gotthardt[1]

Diabetes 2023;72:898–907 | https://doi.org/10.2337/db22-0884

Intrahepatic transplantation of islets of Langerhans (ITx) is a treatment option for individuals with complicated type 1 diabetes and profoundly unstable glycemic control, but its therapeutic success is hampered by deterioration of graft function over time. To improve ITx strategies, technologies to noninvasively monitor the fate and survival of transplanted islets over time are of great potential value. We used [^{68}Ga]Ga-NODAGA-exendin-4 (^{68}Ga-exendin) positron emission tomography (PET)/computed tomography (CT) imaging to demonstrate the feasibility of quantifying β-cell mass in intrahepatic islet grafts in 13 individuals with type 1 diabetes, nine after ITx with functional islet grafts and four control patients not treated with ITx. β-Cell function was measured by mixed-meal tolerance test. With dynamic ^{68}Ga-exendin PET/CT images, we determined tracer accumulation in hepatic hotspots, and intrahepatic fat was assessed using MRI and spectroscopy. Quantification of hepatic hotspots showed a significantly higher uptake of ^{68}Ga-exendin in the ITx group compared with the control group (median 0.55 [interquartile range 0.51–0.63] vs. 0.43 [0.42–0.45]). GLP-1 receptor expression was found in transplanted islets by immunohistochemistry. Intrahepatic fat was not detected in a majority of the individuals. Our study provides the first clinical evidence that radiolabeled exendin imaging can be used to monitor viable transplanted islets after intraportal ITx.

ARTICLE HIGHLIGHTS

- This clinical study researched the potential of radiolabeled exendin to follow the fate and survival of intrahepatic islet grafts.
- Is it feasible to quantitatively detect intrahepatic islet transplants with [^{68}Ga]Ga-NODAGA-exendin-4 (^{68}Ga-exendin) positron emission tomography (PET) imaging?
- Our study findings indicate that the imaging technique ^{68}Ga-exendin PET can be used to monitor viable islet mass after intrahepatic islet transplantation in humans.
- Alongside functional measures, ^{68}Ga-exendin PET imaging could significantly aid in the evaluation of strategies designed to improve islet engraftment, survival, and function.

[1]Department of Medical Imaging, Radboud University Medical Center, Nijmegen, the Netherlands
[2]Department of Nutrition and Movement Sciences, Maastricht University, Maastricht, the Netherlands
[3]Department of Radiology and Nuclear Medicine, Maastricht University Medical Center, Maastricht, the Netherlands
[4]Internal Medicine, Leiden University Medical Center, Leiden, the Netherlands
[5]Internal Medicine, Radboud University Medical Center, Nijmegen, the Netherlands
[6]Internal Medicine, Maastricht University Medical Center, Maastricht, the Netherlands
[7]Internal Medicine, Maxima Medical Center, Veldhoven, the Netherlands
[8]Endocrinology, CHU Lille, Lille, France
[9]Translational Research for Diabetes, Lille, France
[10]Nuclear Medicine, CHU Lille, Lille, France
[11]Department of Medicinal Chemistry, Uppsala University, Uppsala, Sweden

Corresponding author: Marti Boss, marti.boss@radboudumc.nl

Received 25 October 2022 and accepted 3 April 2023

Clinical trial reg. no. NCT03785236, clinicaltrials.gov

This article contains supplementary material online at https://doi.org/10.2337/figshare.22564699.

T.J.P.J. and M.Bu. contributed equally to this work.

Intrahepatic transplantation of islets of Langerhans (ITx) is used in individuals with type 1 diabetes who have severe hypoglycemic episodes along with hypoglycemia unawareness or poorly controlled diabetes (1). The introduction of the Edmonton protocol allowed for successful implementation of this therapy in clinical care (2). Islet transplantation can achieve glycemic control in the nondiabetes range in individuals with type 1 diabetes, with full insulin independence in some, although islets of more than one donor are usually required to achieve this. Nevertheless, graft function often deteriorates over time, and after 5 years, at least 50% of the patients are back on insulin treatment (1,3,4). Despite this reduction in graft function, glycemic control remains better than before ITx in a vast majority of patients (1). Therefore, ITx is a viable approach for selected patients (1,5), although the necessity of immunosuppressive treatment to avoid rejection of the islet transplants and the large number of islets required to treat a single patient, combined with a shortage of donor pancreata/islets, limit the broader application of ITx for the treatment of type 1 diabetes (1). Therefore, the search for improved transplantation strategies and ways to reduce the number of islets needed per transplantation continues (6–10).

To improve ITx strategies, technologies that allow us to follow the fate of transplanted islets are potentially of great value. Currently, islet graft function is assessed using C-peptide and HbA_{1c} (1,4), which may indirectly reflect but do not actually measure β-cell mass (11). Biomedical imaging techniques hold significant promise to quantify islet and, more specifically, β-cell mass after ITx. Such information would aid the advancement of ITx approaches because it would allow us to measure the effect of medical interventions or transplantation/encapsulation strategies on islet survival, in addition to loss of function. MRI and positron emission tomography (PET) using ^{18}F-fluorodeoxyglucose have been proposed for this purpose (12–14), but prelabeling with contrast agents (i.e., superparamagnetic nanoparticles) for MRI might impair islet engraftment (15), and the use of PET tracers for prelabeling does not allow for long-term follow-up of islet grafts because of the radioactive decay of radiotracers.

We have developed and validated a technology that does not depend on prelabeling; it allows specific imaging of viable β-cells using radiolabeled exendin, a glucagon-like peptide 1 (GLP-1) analog (16,17). We previously showed that pancreatic exendin uptake linearly correlates with β-cell mass in rodent models (17–19), and a proof-of-concept study in individuals with type 1 diabetes and healthy volunteers demonstrated reduced pancreatic tracer uptake in those with type 1 diabetes (17,20).

In this study, we aimed to assess the feasibility of quantifying β-cell mass in intrahepatic islet transplants in humans using [^{68}Ga]Ga-NODAGA-exendin-4 (^{68}Ga-exendin) PET imaging.

RESEARCH DESIGN AND METHODS

Study Participants

Thirteen adults with type 1 diabetes were included in the study conducted at the Department of Medical Imaging of Radboud University Medical Center (Radboudumc; Nijmegen, the Netherlands). Twelve individuals were recruited from the diabetes outpatient clinic of Leiden University Medical Center (Leiden, the Netherlands), and one was recruited from Lille University Hospital (CHU de Lille, Lille, France).

Study participants in the ITx group (n = 9) received intrahepatic islet grafts at least 3 months before enrollment. Islet graft function was biochemically proven by stimulated C-peptide >0.8 nmol/L. Participants in the control group (n = 4) were on the waiting list for ITx and had no intrahepatic islet grafts. None of the individuals in either group were or had been treated with synthetic exendin or dipeptidyl-peptidase IV inhibitors. Liver AST and ALT values >135 units/L and chronic kidney disease as defined by an estimated glomerular filtration rate (GFR) <30 mL/min/1.73 m^2 were criteria for exclusion.

All study procedures were performed at Radboudumc. This study was approved by the institutional ethics review committee of Radboudumc, and study participants provided written informed consent before participation. Initially, our intention was to include 10 individuals in the ITx group and five in the control group. This could not be realized because of the small number of individuals who underwent ITx and had islet graft function >0.8 nmol/L or were on the ITx waiting list. Enrollment was also complicated by the closing of research facilities and a temporary stop to enrollment because of the COVID-19 pandemic.

Mixed-Meal Tolerance Test

All individuals underwent a mixed-meal tolerance test (MMTT) to assess β-cell function. The MMTT was performed in the morning, preceded by an overnight 12-h fast, during which only water was consumed. Participants were asked to skip bolus insulin for a period of 6 h before the test. In addition, they were asked to inject approximately two-thirds of the regular long-acting insulin dose or, in case of an insulin pump, to set the basal rate at approximately two-thirds of the default setting. Before the MMTT, blood was drawn to determine fasting glucose, C-peptide, insulin, HbA_{1c}, kidney function, and liver enzymes. Participants consumed 6 mL/kg liquid meal (Nutridrink; Nutricia, Hoofddorp, the Netherlands) to a maximum of 360 mL within 5 min. Blood samples were collected at 0, 15, 30, 60, 90, and 120 min after ingestion to determine stimulated glucose, C-peptide, and insulin.

Glucose levels and basal and stimulated C-peptide levels were used to calculate the area under the curve (AUC) for glucose and C-peptide using Prism 5.03 software (GraphPad Software, Inc., San Diego, CA). To provide a better estimate of β-cell function than $AUC_{C\text{-peptide}}$ alone, the ratio between $AUC_{C\text{-peptide}}$ and $AUC_{glucose}$ was calculated. The

ratio of $AUC_{C\text{-peptide}}$ to $AUC_{glucose}$ and peak C-peptide measurements were then correlated with the results of the image analysis for each participant.

PET/Computed Tomography Acquisition

Image acquisition was performed on a Siemens Biograph 40 mCT time-of-flight PET/computed tomography (CT) system (effective resolution ~3–4 mm). PET/CT acquisition for one of the control patients was unsuccessful because of a system failure. Participants fasted for at least 4 h before the PET examination, and insulin use was temporarily adjusted similar to the preparation for the MMTT. Dynamic PET images were acquired for 60 min starting immediately after a 100-s intravenous infusion of 1.2 MBq/kg ^{68}Ga-exendin (peptide dose 4–7 μg). Radiochemical preparation was performed as previously described (16). Image data were obtained with one bed position that included the liver in the field of view. For anatomical information and attenuation correction, low-dose CT without contrast of the abdomen was acquired.

Hotspot Analysis

Reconstructed PET/CT data were analyzed using PMOD version 3.508 software (PMOD Technologies, Zurich, Switzerland). The low-dose CT scan was used for the complete manual delineation of the hepatic volume. A cylindrical volume of interest (VOI) was placed fully in the lumen of the abdominal descending aorta to obtain an image-derived input function for the Logan plot, a graphical analysis technique (21). A spherical VOI was positioned in the erector spinae muscle to measure the background level of the tracer. Because exendin accumulation in the kidneys is high (16), and the right kidney is in the proximity of the liver, the spillover in the peripheral part of the liver was excluded from the hepatic VOI.

The standardized uptake value (SUV) in the liver of control patients was determined and averaged, resulting in a group average (hepatic $SUV_{controls}$). This was assumed to correspond to background uptake of ^{68}Ga-exendin. A cutoff level was then determined consisting of the hepatic $SUV_{controls}$ plus twice the SD, as earlier described (22). This cutoff level (hepatic $SUV_{controls}$ + 2SD = 1.7) was applied to all patients to identify hotspots with hepatic tracer uptake above this level. Subsequently, these hotspots within the hepatic volume were automatically identified and segmented by isocontouring. The dynamic uptakes of ^{68}Ga-exendin during all frames of the PET scan were then extracted for each individual and used as input for the Logan plot in the kinetic modeling module in PMOD (PKIN; PMOD Technologies). The blood signal as determined from the descending aorta was used as input function. The Logan plot allows the estimation of the total distribution volume (V_T) of the tracer (21). The V_T is defined as the ratio between the radiotracer concentration in target tissue (kBq/cm^3) to that in plasma (kBq/mL) at equilibrium and thus provides information on the rate of the radiotracer uptake in the target tissue, compared to the background circulating tracer in blood. The combination of hotspot localization and information on tracer kinetics in those areas provides insight into tracer accumulation in intrahepatic islet grafts. The analysis of the dynamic PET data was performed as described in a previous study (22).

Immunohistochemistry

One of the patients treated with transplantation (ITx9) underwent a surgical liver biopsy at the time of a laparoscopic cholecystectomy performed for a symptomatic gallstone, 24 months after the last islet infusion. After fixation in formalin (formaldehyde 4%; Sigma-Aldrich, Saint Quentin Fallavier, France), sections of the liver tissue were immunostained for GLP-1 receptor (Developmental Studies Hybridoma Bank ref. no. monoclonal antibody 3F52 4ea 12/5/19 anti-mouse) and insulin diluted at 1/1,000 (Abcam ref. no. ab181547 anti-rabbit). After deparaffinization and rehydration of the paraffin sections, pretreatment in microwave was performed as described by Waser et al. (23). The slides were incubated overnight at 4°C with the primary GLP-1 receptor antibody, and after revelation, the anti-insulin antibody was incubated for 2 h at room temperature. GLP-1 receptor was revealed with secondary Alexa Fluor 594 (anti-mouse AF-594; cat. no. 11032; Invitrogen) and insulin with Alexa Fluor 488 (anti-rabbit AF-488; cat. no. 21206; Invitrogen) diluted at 1/800 and applied for 1 h at room temperature.

Intrahepatic Fat Content

A Dixon sequence was used to map fat deposition in the liver. Hotspots identified on PET were compared with the mapped fat deposition to look for possible matches. In addition, the Dixon scan was used to qualitatively assess the presence of hepatic steatosis.

Proton magnetic resonance spectroscopy (^{1}H-MRS) was used to quantify hepatic lipid content. Spectra were obtained from a voxel positioned in the liver avoiding large vessels during a single breath hold in expiration. The MRS spectrum was obtained without water suppression. All MR experiments were performed on a 3 Tesla Siemens MR system (3T Magnetom Skyra; Siemens, Erlangen, Germany) using an 18-channel body-phased array coil positioned on the abdomen in combination with a 32-channel spine coil.

Postprocessing of the MRS data was performed by time-domain fitting using the AMARES quantification option in the software package jMRUI (www.jmrui.eu). Intrahepatic fat was estimated by calculating the relative lipid content, which was defined as the signal intensity of the methylene lipid signal at 1.33 parts per million, divided by the sum of the signal intensity of the methylene lipid signal and water signal at 4.7 parts per million (Eq. 1). Intrahepatic fat content >5.6% was defined as hepatic steatosis (24). Because of excessive movement, one

scan could not be used for quantification. For technical specifications on imaging and spectroscopy, see Supplementary Material.

$$Intrahepatic\ fat\ (\%) = \frac{lipid}{lipid + H_2O} \times 100\ (\%) \quad (1)$$

Statistical Analysis

Acquired data of the groups are expressed as mean ± SD or median (interquartile range [IQR]). The Mann-Whitney *U* test was used to assess group differences, and data are shown as median (IQR). Correlations between V_T and ratio of $AUC_{C\text{-}peptide}$ to $AUC_{glucose}$ and islet equivalents (IEQs) were analyzed by the Pearson correlation coefficient (*r*) with a two-tailed ANOVA. The level of significance was set at $P < 0.05$. GraphPad Prism software was used for all analyses (GraphPad Prism 5 for Windows).

Data and Resource Availability

The data sets generated during and/or analyzed during the current study are available from the corresponding author on reasonable request.

RESULTS

Patient age, BMI, diabetes duration, and renal function were comparable between the two groups (Table 1). Individuals treated with ITx underwent one or more islet transplantations within 5 years before enrollment, and the number of transplanted islets ranged from 0.5 to 1.3 million IEQs. Of these nine individuals treated with ITx, five were insulin independent at the time of ^{68}Ga-exendin PET imaging. Compared with patients not undergoing transplantation, those treated with ITx had significantly lower HbA_{1c} (P = 0.02), higher stimulated peak C-peptide values (P = 0.003), and a higher ratio of $AUC_{C\text{-}peptide}$ to $AUC_{glucose}$ (P = 0.003) determined in the MMTT (Table 1). One of the participants was scanned twice, once before ITx and once 9 months after (Table 1). In this participant, HbA_{1c} fell from 7.7 (61 mmol/mol) to 6.5% (47 mmol/mol), and stimulated peak C-peptide and ratio of $AUC_{C\text{-}peptide}$ to $AUC_{glucose}$ increased from 0.42 to 2.17 nmol/L and 0.02 to 0.20 nmol · min/L, respectively.

After injection of ^{68}Ga-exendin, two patients experienced nausea and vomiting. No other adverse events related to study procedures were observed. One participant was hospitalized because of pneumonia, but this was deemed unrelated to study procedures.

Figure 1*A* shows an example of a transaxial projection from a ^{68}Ga-exendin PET/CT scan displaying distinct regions with strong hepatic uptake. The hepatic $SUV_{controls}$ was 1.3 ± 0.2, which was in line with the hepatic SUV determined in a ventral VOI in individuals with type 1 diabetes from a previous study (0.86 ± 0.25) (25). Using a hepatic $SUV_{controls}$ + 2SD resulted in a cutoff value of 1.7. Regional uptake above this threshold value was defined as a hotspot. The V_T of ^{68}Ga-exendin within defined hotspots was significantly higher in patients treated with ITx than in control patients (median 0.55 [IQR 0.51–0.63] vs. 0.43 [0.42–0.45]; P = 0.009) (Fig. 1*B*). The individual who was scanned twice showed an increase in V_T from 0.45 to 0.53 (Fig. 1*B*). No correlation was found between the V_T of the tracer and the IEQs of the transplant (Pearson r = 0.18; P = 0.64) nor between the V_T and the ratio of $AUC_{C\text{-}peptide}$ to $AUC_{glucose}$ (Pearson r = 0.15; P = 0.70) (Fig. 2*A* and *B*).

In all patients, multiple hepatic hotspots were found on the PET images through qualitative assessment, except in one control patient showing no hotspots on the PET scan (participant C4). The ITx group had a numerically higher number of hotspots (5.9 ± 4.3; total 53) than the control group (2.0 ± 2.0; total 6), but this difference failed to reach statistical significance (P = 0.11).

In the patient who underwent liver biopsy 24 months after the last ITx, immunohistochemical analyses of the biopsy tissue indicated the presence of insulin-positive cell clusters (Fig. 3). Anti–GLP-1 receptor staining showed that these insulin-positive cells expressed the GLP-1 receptor, which is required for exendin uptake.

To study whether the presence of islet mass correlates with regions with enhanced lipid content in the liver, we sought to map hepatic liver fat distribution using a modified Dixon sequence and compare these MR scans with the locations of the identified hotspots on the PET images (Fig. 4). Based on the Dixon maps, regions of enhanced fat deposition were identified in two patients treated with ITx and one control patient. Each fat deposition in these patients matched with hotspots identified on the PET images. Furthermore, the Dixon scans were used to qualitatively assess hepatic steatosis, which was observed on both examinations in the individual who was scanned twice and, in another patient, treated with ITx. These patients were, however, different from the individuals who had fat depositions in the liver. Based on these findings, no clear relationship between the PET hotspots and hepatic fat depositions on Dixon scans could be observed.

Intrahepatic fat was also determined with another approach, ^{1}H-MRS, and was expressed as the relative lipid content (Eq. 1). An overview of the results can be found in Table 2. All individuals had a normal quantity of intrahepatic fat (≤5.6%) except one participant in the ITx group. This patient with high intrahepatic fat content also demonstrated hepatic steatosis on the Dixon scan. Figure 5 illustrates the ^{1}H-MR spectrum of normal and high quantities of intrahepatic fat. There was no difference in intrahepatic fat between the ITx and control groups (P = 0.86).

DISCUSSION

Here, we provide the first clinical evidence that ^{68}Ga-labeled exendin uptake can be used for quantification and monitoring of intraportally transplanted islets.

Table 1—Clinical characteristics of individuals with biochemically proven functional intrahepatic islet grafts (ITx; *n* = 9) and those awaiting islet transplantation with no intrahepatic islet grafts (control; *n* = 4)

	Age, years	BMI, kg/m^2	Sex	Diabetes duration, years	HbA_{1c}, % (mmol/mol)	CKD-EPI GFR, mL/min/1.73 m^2	AST/ALT, units/L	Mean blood glucose week before PET/CT scan, mmol/L	Basal glucose, mmol/L	Stimulated C-peptide peak, nmol/L	IEQs/*n* of donors	Time since ITx, months
ITx												
ITx1	58	23.0	M	51	5.7 (39)	40	29/18	—	6.4	1.97	1,088,010/2	62
ITx2	52	19.6	F	45	6.5 (47)	62	19/13	4.7	6.9	2.32	1,200,000/2	39
ITx3	66	21.7	M	53	8.3 (67)	>90	52/71	6.6	10.2	1.03	710,000/3	6
ITx4*	54	21.5	F	36	5.4 (36)	33	27/18	5.8	4.4	1.62	1,300,000/2	68
ITx5	40	23.0	F	39	5.6 (38)	55	23/17	7.0	7.3	1.83	479,000/1	17
ITx6	64	30.8	F	48	6.2 (44)	49	64/61	—	6.9	1.72	1,152,283/3	15
ITx7	59	25.9	M	47	6.9 (52)	41	16/13	6.7	5.3	0.85	869,565/2	17
ITx8	68	28.1	M	38	6.5 (47)	42	21/20	6.4	5.2	2.17	729,000/2	9
ITx9†	56	21.9	F	54	5.7 (39)	69	19/13	—	4.6	2.09	842,559/3	27
Group	58 ± 9	23.9 ± 3.6	4 M/5 F	46 ± 7	6.3 ± 0.9 (45 ± 10)	53 ± 18	30 ± 17/27 ± 22	6.2 ± 0.8	6.4 ± 1.8	1.73 ± 0.50	930,046 ± 271,034	29 ± 24
Control												
C1	65	27.3	M	35	7.7 (61)	54	18/18	8.8	8.7	0.42	—	—
C2	56	26.9	M	46	8.5 (69)	65	25/26	11.8	4.0	0.26	—	—
C3‡	59	27.0	M	28	8.6 (70)	55	23/29	—	15.0	0.32	—	—
C4	55	19.3	F	40	7.4 (57)	49	42/31	—	5.2	0.03	—	—
Group	59 ± 5	25.1 ± 3.9	3 M/1 F	37 ± 8	8.1 ± 0.6 (64 ± 6)	56 ± 7	27 ± 10/26 ± 6	10.3	8.2 ± 4.9	0.26 ± 0.17	—	—

Data given as mean ± SD. One study participant was first in the control group (C1) and later received intrahepatic islet grafts (ITx8). CKD-EPI, Chronic Kidney Disease Epidemiology Collaboration. *No MR data available. †Hepatic tissue was available for immunohistochemistry. ‡No PET/CT data available.

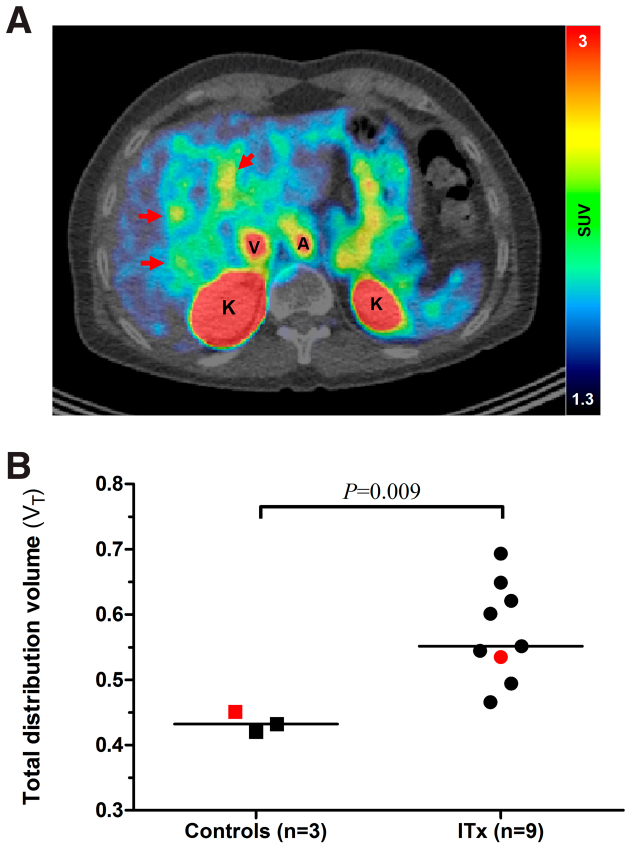

Figure 1—Quantification of PET/CT images. *A*: Hepatic regions with high tracer uptake on PET, illustrated in the transversal PET/CT image of participant ITx9 (indicated by red arrows). Other regions with high uptake are the kidneys (K), abdominal aorta (A), and inferior vena cava (V). *B*: V_T was determined for control and ITx groups. The individual who was imaged both before and after transplantation is identified by symbols in red.

Quantification of the identified hepatic hotspots demonstrated a higher uptake of ^{68}Ga-exendin in individuals with transplanted islets than in individuals not treated with ITx. Circulating C-peptide was higher in individuals treated with ITx, which proved the functionality of the islet grafts. In addition, in one patient treated with ITx, GLP-1 receptor expression was demonstrated in islet grafts in liver tissue by immunohistochemistry.

We observed no correlation between the V_T of ^{68}Ga-exendin in the identified hotspots and the IEQs of the transplant. Based on data from ^{18}F-fluorodeoxyglucose–labeled islets, a majority of intrahepatically transplanted islets fail to engraft and die shortly after transplantation (14). Furthermore, a large individual variability in graft survival in the peritransplantation period has been demonstrated. Because imaging was performed 6 to 68 months after transplantation, the transplanted IEQs do not necessarily reflect the viable islet mass at the time point of scanning (17), explaining the lack of correlation of exendin uptake with administered IEQs. Also, the V_T of ^{68}Ga-exendin did not directly correlate with functional parameters, which is not surprising, considering that the presence of viable β-cells does not necessarily mean that these cells are functional (or function equally well) (20,26,27). Our observations highlight the importance of an imaging biomarker reflecting β-cell mass to complement functional measures of islet graft performance.

Among the clinically available tracers to date, radiolabeled exendin-4 offers the highest sensitivity and specificity for β-cells (17–19,28–30). It is one of the few islet cell tracers that have been evaluated in clinical trials, with [^{11}C]C-5-HTP being the only other method having been used to monitor intraportally transplanted islet grafts (22). However, [^{11}C]C-5-HTP is a biomarker for endocrine cells rather than specifically for β-cells because uptake and retention are mediated by the serotonin biosynthesis pathway present in most endocrine tissues, including all islet cell subtypes (31). The potential of exendin to image transplanted human β-cells has been previously suggested with planar scintigraphy after intramuscular islet autotransplantation (32). Exendin is β-cell specific because of the strong expression of the GLP-1 receptor on β-cells. Although some GLP-1 receptor expression has been reported in islet δ-cells (33), these cells account for maximally 5% of islet mass (34,35), and potential overestimation of β-cell mass as a result of exendin uptake in δ-cells is most likely not relevant. Ductal cells can express the GLP-1 receptor as

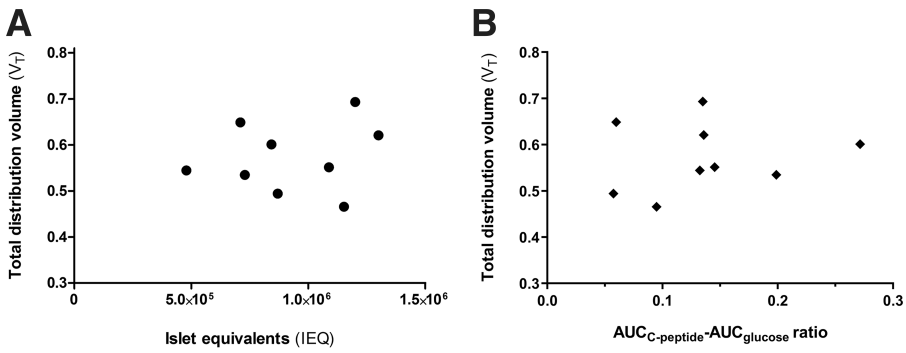

Figure 2—Correlations with V_T. *A*: Correlation between IEQs and V_T in the ITx group (n = 9; Pearson r = 0.18; P = 0.64). *B*: Correlation between the ratio of $AUC_{C\text{-peptide}}$ to $AUC_{glucose}$ and V_T (Pearson r = 0.15; P = 0.70).

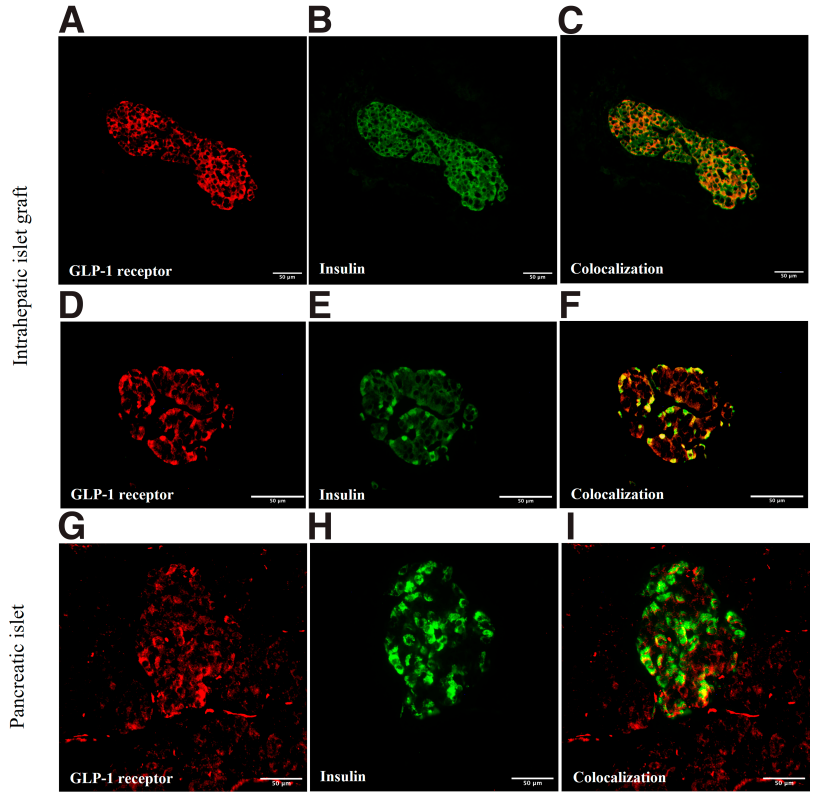

Figure 3—*A–I*: Immunohistochemistry images of hepatic tissue after ITx (*A–F*) compared with pancreatic tissue (control) (*G–I*). Immunohistochemical analysis of hepatic tissue sections from a patient treated with ITx (ITx9) showing the presence of GLP-1 receptor expression on insulin-positive cell clusters. The hepatic tissue sections that were stained for the GLP-1 receptor and insulin showed colocalization (*C* and *F*), similar to the pancreatic tissue sections used as control (*I*).

well, but the expression level is even lower than that in δ-cells (33), and because these cells are spread out over the whole organ, they will only mildly contribute to background activity.

To reliably quantify the uptake of ^{68}Ga-exendin in intrahepatic islets grafts, we used a previously described method (22) that reduces the influence of background signal and improves the detection of focal accumulations of islets in the liver, indicated by the significant increase in V_T of the tracer in the hotspots of patients treated with ITx. In addition, because radiolabeled exendin is cleared via the kidneys (36), substantial differences in GFR might influence tracer distribution and uptake. To mitigate this potential impact, we excluded individuals with an estimated GFR <30 mL/min/1.73 m^2 and included control patients with comparable kidney function. The focal distribution pattern we observed in the liver was in line with previous studies demonstrating an uneven islet distribution rather than a homogeneous distribution across the liver (14,37). Besides the background uptake in the blood pool, some receptor-mediated tracer uptake might theoretically also occur because human hepatocytes can express low levels of the GLP-1 receptor (38). However, in a previous study with 62 participants (including those with type 1 and type 2 diabetes), no uptake of ^{68}Ga-labeled exendin was observed in the liver (39). Similarly, ^{68}Ga-DOTA–labeled exendin-4 demonstrated hepatic uptake lower than that of blood in individuals with type 2 diabetes (40). The low background activity in the liver renders our approach a sensitive and reliable technique for detecting GLP-1 receptor–rich islet grafts.

For an imaging biomarker to reflect true β-cell mass, expression of the target needs to be stable and should not be affected by physiological or metabolic changes. A concern when using exendin can be the stability of GLP-1 receptor expression and its effect on image quantification (41). However, our preclinical validation studies have demonstrated that exendin uptake in islets is reproducible (42); it linearly correlates with β-cell mass (17–19,28), and uptake is not affected by inflammatory processes (18,19). The latter is of particular relevance because type 1 diabetes is an autoimmune disease, and recurrence of autoimmunity after ITx is one of the factors associated with loss of graft function (4). Only high blood glucose levels have been demonstrated in humans to downregulate GLP-1 receptor expression (43,44) and thus exendin uptake in human islets, an effect that is restored after normalization of blood glucose levels (41). None of the individuals in the present study experienced severely elevated blood glucose levels in the week before imaging,

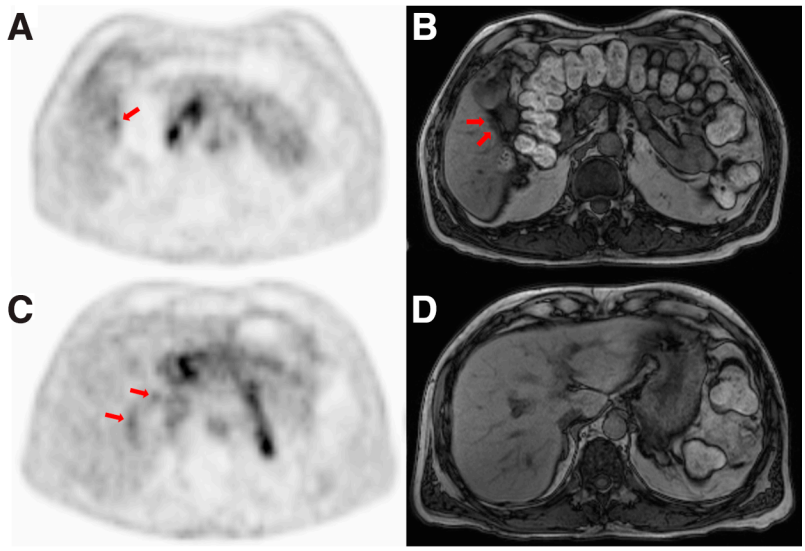

Figure 4—Qualitative assessment of PET and MR images. *A–D*: PET and MR images of study participant ITx1 (axial views). Multiple hotspots on the exendin PET scan were found (indicated by red arrows) (*A* and *C*). Colocalization was found between the position of a hotspot on the exendin PET image (red arrow) (*A*) and a fat deposition on the MR image using the Dixon sequence (red arrows) (*B*). No other colocalizations were found in this study, illustrated by two hotspots found on the PET image (*C*) but with no fat depositions on the corresponding MR image (*D*).

and five of nine individuals treated with ITx were insulin independent.

Another important aspect that should be considered is radiation exposure, in particular, radiation to the islets. Dosimetry studies of ^{68}Ga-exendin have demonstrated that the pancreatic islet–absorbed dose clearly remained <2 mGy. Considering that the risk of diabetes increases in adults receiving more than ~10 Gy to the islets, with higher sensitivity in children (45,46), the radiation exposure of ^{68}Ga-exendin PET remains more than 5,000 times lower, so even multiple PET/CT scans could be performed in adults annually without risk (16).

Table 2—Intrahepatic fat of study participants in control and ITx groups

Study participant	Intrahepatic fat, %
ITx	
ITx1	0.9
ITx2	0.8
ITx4	3.3
ITx5	0.8
ITx6	27.4
ITx7	0.6
ITx8	2.0
ITx9	1.8
Group (*n* = 8)	1.35 (0.80–2.98)
Control	
C1	1.0
C2	2.1
C3	1.1
C4	0.6
Group (*n* = 4)	1.05 (0.70–1.85)

Group values given as median (IQR). Of these 12 participants, 11 fell within the normal category (≤5.6%) (24). Only one participant from the ITx group (ITx6) was considered to have abnormal intrahepatic fat content (>5.6%), with an estimated intrahepatic fat of 27.4%.

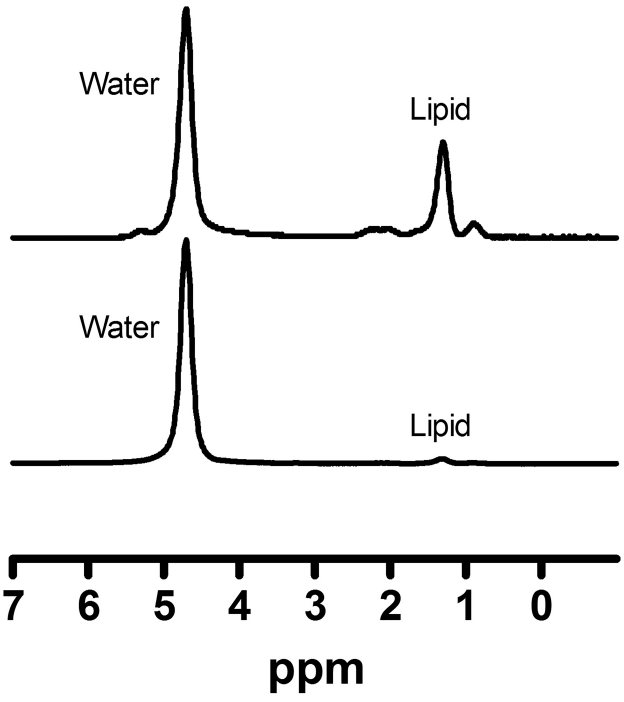

Figure 5—Hepatic MR proton spectra. MR proton spectra of the livers of two individuals from the ITx group. The upper spectrum originates from participant ITx6, with the overall highest intrahepatic fat (27.4%), and the lower spectrum from participant ITx8, with 2.0% intrahepatic fat. The water proton signal is marked as water, and the lipid methylene proton signal as lipid. The resonance frequencies are indicated on the horizontal axis: 4.7 parts per million (ppm) for water and 1.33 ppm for lipid.

Insulin secreted by transplanted islets can promote local fat deposition by focal hyperinsulinism caused by hypersecreting islet grafts (1,47–49). Therefore, we hypothesized that accumulation of ^{68}Ga-exendin may coincide with local fat deposition in the liver. We indeed found that the number of hepatic hotspots was almost ninefold higher in the ITx group, but colocalizations between hotspots and focal fat deposition could be demonstrated only in three individuals, including one control patient. Therefore, liver fat depositions and hotspots did not colocalize as hypothesized, which may have been due to limited spatial resolution and sensitivity of the imaging techniques. Also, it is possible that fat depositions reside in areas where islets initially engrafted but were later lost, leaving just the fat deposition and no viable islets (and thus no radiotracer uptake). Finally, hepatic steatosis can be a reversible process, and only hotspots on PET would then be visible, without fat depositions (48,50,51). Hepatic steatosis was observed in the individual who was examined before and after ITx and in the patient treated with ITx with the highest percentage of intrahepatic fat on ^{1}H-MRS. There was, however, no apparent relation between ITx and hepatic steatosis. Intrahepatic fat was also measured with ^{1}H-MRS but was not different between the groups.

In conclusion, our study indicates that radiolabeled exendin imaging can be used to monitor viable islet mass after intrahepatic islet transplantation in humans. Ideally, ^{68}Ga-exendin PET imaging might be used alongside functional measures. Combined, these parameters could significantly aid the evaluation of strategies designed to improve islet engraftment, survival, and function.

Acknowledgments. The authors thank the technicians for their assistance and help with the PET/CT acquisitions, MRI, and ^{1}H-MRS. The authors also thank the laboratory technicians for their help with the radiolabeling and assistance in the laboratory. The authors express their greatest gratitude to the study participants for their valuable contribution.

Funding. This work is supported by BetaCure (FP7/2014–2018; grant 602812) and the Diabetes Foundation The Netherlands Fellowship (2015-81-1845). This work is also supported by IMI2-JU under grants 115797 (INNODIA) and 948268 (INNODIA HARVEST). This joint undertaking receives support from the Union's Horizon 2020 Research and Innovation Program as well as the European Federation of Pharmaceutical Industries and Associations, JDRF, and the Leona M. and Harry B. Helmsley Charitable Trust. O.E.'s position is supported by the Science for Life Laboratory and the Swedish Research Council (2020-02312).

Duality of Interest. O.E. is an employee of Antaros Medical AB and a cofounder of Antaros Tracer AB. No other potential conflicts of interest relevant to this article were reported.

Author Contributions. T.J.P.J. drafted the manuscript with the assistance of M.Bu. T.J.P.J., M.Bu., M.Bo., and M.v.d.G. helped with the conduct of the study. T.J.P.J., M.Bu., M.v.d.G., S.v.K., M.-C.V., A.B., F.P., I.V., O.E., and M.G. performed data analysis. M.Bu., M.Bo., M.Br., B.E.d.G., M.A.E., O.E., E.J.P.d.K., and M.G. contributed to conception and design. M.F.N. performed patient screening. All authors contributed to the interpretation of the acquired data. All authors were involved in the revision process and approved the final version. M.G. is the guarantor of this work and, as such, had full access to all the data in the study and takes responsibility for the integrity of the data and the accuracy of the data analysis.

Prior Presentation. Parts of this work were given as oral presentations at the Annual Meeting for North Europe Young Diabetologists, Lyngby, Denmark, 8–10 May 2019, and the Annual Congress of the European Association of Nuclear Medicine, 22–30 October 2020. Parts of this work were also presented as poster presentations at the European Molecular Imaging Meeting, Glasgow, Scotland, 19–22 March 2019; the Annual Meeting of the European Association for the Study of Diabetes (EASD), Barcelona, Spain, 16–20 September 2019; and the Annual Meeting of the EASD, 21–25 September 2020.

References

1. Vantyghem MC, de Koning EJP, Pattou F, Rickels MR. Advances in β-cell replacement therapy for the treatment of type 1 diabetes. Lancet 2019;394:1274–1285

2. Shapiro AM, Lakey JR, Ryan EA, et al. Islet transplantation in seven patients with type 1 diabetes mellitus using a glucocorticoid-free immunosuppressive regimen. N Engl J Med 2000;343:230–238

3. Shapiro AM, Pokrywczynska M, Ricordi C. Clinical pancreatic islet transplantation. Nat Rev Endocrinol 2017;13:268–277

4. Rickels MR, Robertson RP. Pancreatic islet transplantation in humans: recent progress and future directions. Endocr Rev 2019;40:631–668

5. Foster ED, Bridges ND, Feurer ID, Eggerman TL, Hunsicker LG; Clinical Islet Transplantation Consortium. Improved health-related quality of life in a phase 3 islet transplantation trial in type 1 diabetes complicated by severe hypoglycemia. Diabetes Care 2018;41:1001–1008

6. Pullen LC. Stem cell-derived pancreatic progenitor cells have now been transplanted into patients: report from IPITA 2018. Am J Transplant 2018;18:1581–1582

7. Baidal DA, Ricordi C, Berman DM, et al. Bioengineering of an intraabdominal endocrine pancreas. N Engl J Med 2017;376:1887–1889

8. Ludwig B, Ludwig S, Steffen A, et al. Favorable outcome of experimental islet xenotransplantation without immunosuppression in a nonhuman primate model of diabetes. Proc Natl Acad Sci USA 2017;114:11745–11750

9. Odorico J, Markmann J, Melton D, et al. Report of the key opinion leaders meeting on stem cell-derived beta cells. Transplantation 2018;102:1223–1229

10. Ekser B, Ezzelarab M, Hara H, et al. Clinical xenotransplantation: the next medical revolution? Lancet 2012;379:672–683

11. Oram RA, Sims EK, Evans-Molina C. Beta cells in type 1 diabetes: mass and function; sleeping or dead? Diabetologia 2019;62:567–577

12. Wang P, Schuetz C, Vallabhajosyula P, et al. Monitoring of allogeneic islet grafts in nonhuman primates using MRI. Transplantation 2015;99:1574–1581

13. Gálisová A, Herynek V, Swider E, et al. A trimodal imaging platform for tracking viable transplanted pancreatic islets in vivo: F-19 MR, fluorescence, and bioluminescence imaging. Mol Imaging Biol 2019;21:454–464

14. Eriksson O, Eich T, Sundin A, et al. Positron emission tomography in clinical islet transplantation. Am J Transplant 2009;9:2816–2824

15. Sakata N, Yoshimatsu G, Tsuchiya H, et al. Imaging of transplanted islets by positron emission tomography, magnetic resonance imaging, and ultrasonography. Islets 2013;5:179–187

16. Boss M, Buitinga M, Jansen TJ, Brom M, Visser EP, Gotthardt M. PET-based human dosimetry of 68Ga-NODAGA-exendin-4, a tracer for β-cell imaging. J Nucl Med 2020;61:112–116

17. Brom M, Woliner-van der Weg W, Joosten L, et al. Non-invasive quantification of the beta cell mass by SPECT with ^{111}In-labelled exendin. Diabetologia 2014;57:950–959

18. Brom M, Joosten L, Frielink C, et al. Validation of ^{111}In-exendin SPECT for the determination of the β-cell mass in BioBreeding diabetes-prone rats. Diabetes 2018;67:2012–2018

19. Joosten L, Brom M, Peeters H, et al. Measuring the pancreatic β cell mass in vivo with exendin SPECT during hyperglycemia and severe insulitis. Mol Pharm 2019;16:4024–4030

20. Boss M, Kusmartseva I, Woliner-van der Weg W, et al. 111In-exendin SPECT imaging suggests presence of residual beta cells in patients with longstanding type 1 diabetes (Abstract). Diabetologia 2020;63(Suppl. 1):43
21. Logan J, Fowler JS, Volkow ND, et al. Graphical analysis of reversible radioligand binding from time-activity measurements applied to [N-11C-methyl]-(-)-cocaine PET studies in human subjects. J Cereb Blood Flow Metab 1990; 10:740–747
22. Eriksson O, Selvaraju R, Eich T, et al. Positron emission tomography to assess the outcome of intraportal islet transplantation. Diabetes 2016;65: 2482–2489
23. Waser B, Blank A, Karamitopoulou E, Perren A, Reubi JC. Glucagon-like-peptide-1 receptor expression in normal and diseased human thyroid and pancreas. Mod Pathol 2015;28:391–402
24. Szczepaniak LS, Nurenberg P, Leonard D, et al. Magnetic resonance spectroscopy to measure hepatic triglyceride content: prevalence of hepatic steatosis in the general population. Am J Physiol Endocrinol Metab 2005;288: E462–E468
25. Jansen TJP, Brom M, Boss M, et al. Importance of beta cell mass for glycaemic control in people with type 1 diabetes. Diabetologia 2023;66: 367–375
26. Keenan HA, Sun JK, Levine J, et al. Residual insulin production and pancreatic β-cell turnover after 50 years of diabetes: Joslin Medalist Study. Diabetes 2010;59:2846–2853
27. Yu MG, Keenan HA, Shah HS, et al. Residual β cell function and monogenic variants in long-duration type 1 diabetes patients. J Clin Invest 2019;129: 3252–3263
28. Brom M, Joosten L, Frielink C, Boerman O, Gotthardt M. (111)In-exendin uptake in the pancreas correlates with the β-cell mass and not with the α-cell mass. Diabetes 2015;64:1324–1328
29. Eriksson O, Laughlin M, Brom M, et al. In vivo imaging of beta cells with radiotracers: state of the art, prospects and recommendations for development and use. Diabetologia 2016;59:1340–1349
30. Eter WA, Van der Kroon I, Andralojc K, et al. Non-invasive in vivo determination of viable islet graft volume by ^{111}In-exendin-3. Sci Rep 2017;7: 7232
31. Eriksson O, Espes D, Selvaraju RK, et al. Positron emission tomography ligand [11C]5-hydroxy-tryptophan can be used as a surrogate marker for the human endocrine pancreas. Diabetes 2014;63:3428–3437
32. Pattou F, Kerr-Conte J, Wild D. GLP-1-receptor scanning for imaging of human beta cells transplanted in muscle. N Engl J Med 2010;363:1289–1290
33. Segerstolpe Å, Palasantza A, Eliasson P, et al. Single-cell transcriptome profiling of human pancreatic islets in health and type 2 diabetes. Cell Metab 2016;24:593–607
34. Wright JJ, Saunders DC, Dai C, et al. Decreased pancreatic acinar cell number in type 1 diabetes. Diabetologia 2020;63:1418–1423
35. Arrojo E Drigo R, Jacob S, García-Prieto CF, et al. Structural basis for delta cell paracrine regulation in pancreatic islets. Nat Commun 2019;10:3700
36. Vegt E, van Eerd JEM, Eek A, et al. Reducing renal uptake of radiolabeled peptides using albumin fragments. J Nucl Med 2008;49:1506–1511
37. Toso C, Vallee JP, Morel P, et al. Clinical magnetic resonance imaging of pancreatic islet grafts after iron nanoparticle labeling. Am J Transplant 2008; 8:701–706
38. Gupta NA, Mells J, Dunham RM, et al. Glucagon-like peptide-1 receptor is present on human hepatocytes and has a direct role in decreasing hepatic steatosis in vitro by modulating elements of the insulin signaling pathway. Hepatology 2010;51:1584–1592
39. Deden L, Boss M, Hazebroek E, Gotthardt M. Imaging the GLP-1 receptor in human by using radiolabeled exendin-4 PET/CT. In The NASO Scientific Spring Meeting Abstract Book 2022, Utrecht, the Netherlands, Netherlands Association for the Study of Obesity, p. 7
40. Eriksson O, Velikyan I, Haack T, et al. Imaging of the glucagon receptor in subjects with type 2 diabetes. J Nucl Med 2021;62:833–838
41. Buitinga M, Cohrs CM, Eter WA, et al. Noninvasive monitoring of glycemia-induced regulation of GLP-1R expression in murine and human islets of Langerhans. Diabetes 2020;69:2246–2252
42. Eter WA, Bos D, Frielink C, Boerman OC, Brom M, Gotthardt M. Graft revascularization is essential for non-invasive monitoring of transplanted islets with radiolabeled exendin. Sci Rep 2015;5:15521
43. Xu G, Kaneto H, Laybutt DR, et al. Downregulation of GLP-1 and GIP receptor expression by hyperglycemia: possible contribution to impaired incretin effects in diabetes. Diabetes 2007;56:1551–1558
44. Rajan S, Dickson LM, Mathew E, et al. Chronic hyperglycemia downregulates GLP-1 receptor signaling in pancreatic β-cells via protein kinase A. Mol Metab 2015;4:265–276
45. van der Kroon I, Woliner-van der Weg W, Brom M, et al. Whole organ and islet of Langerhans dosimetry for calculation of absorbed doses resulting from imaging with radiolabeled exendin. Sci Rep 2017;7:39800
46. de Vathaire F, El-Fayech C, Ben Ayed FF, et al. Radiation dose to the pancreas and risk of diabetes mellitus in childhood cancer survivors: a retrospective cohort study. Lancet Oncol 2012;13:1002–1010
47. Venturini M, Maffi P, Querques G, et al. Hepatic steatosis after islet transplantation: can ultrasound predict the clinical outcome? A longitudinal study in 108 patients. Pharmacol Res 2015;98:52–59
48. Bhargava R, Senior PA, Ackerman TE, et al. Prevalence of hepatic steatosis after islet transplantation and its relation to graft function. Diabetes 2004;53:1311–1317
49. Maffi P, Angeli E, Bertuzzi F, et al. Minimal focal steatosis of liver after islet transplantation in humans: a long-term study. Cell Transplant 2005;14: 727–733
50. Shapiro AM. Islet transplantation in type 1 diabetes: ongoing challenges, refined procedures, and long-term outcome. Rev Diabet Stud 2012;9:385–406
51. Markmann JF, Rosen M, Siegelman ES, et al. Magnetic resonance-defined periportal steatosis following intraportal islet transplantation: a functional footprint of islet graft survival? Diabetes 2003;52:1591–1594